The Casimir energy of skyrmions in the 2+1-dimensional $O(3)$-model

H. Walliser and G. Holzwarth

Fachbereich Physik, Universität Siegen, D57068 Siegen, Germany

Abstract

One-loop quantum corrections to the classical vortices in 2+1 dimensional $O(3)$-models are evaluated. Skyrme and Zeeman potential terms are used to stabilize the size of topological solitons. Contributions from zero modes, bound–states and scattering phase–shifts are calculated for vortices with winding index $n = 1$ and $n = 2$. For both cases the S-matrix shows a pronounced series of resonances for magnon-vortex scattering in analogy to the well-established baryon resonances in hadron physics, while vortices with $n > 2$ are already classically unstable against decay. The quantum corrections destabilize the classically bound $n = 2$ configuration. Approximate independence of the results with respect to changes in the renormalization scale is demonstrated.

PACS 12.39.Dc, 12.39.Fe, 75.30.Ds, 75.50.Ee
Keywords: skyrmions, $O(3)$-model

1 Introduction

Effective field theories have found increasing interest as powerful tools for describing the dynamics of physical systems where global symmetries are spontaneously broken and continuous order parameter fields represent the relevant low-energy degrees of freedom. Depending on space dimensionality and the manifold on which the fields live classical localized static solutions may fall into topologically distinct classes characterized by integer winding numbers, carrying energy, momentum and internal properties which suggest their interpretation as particle-like excitations of the uniform ground state. Their spatial size is determined by scaling properties of different competing terms in the effective lagrangian.

Quantization of effective field theories allows to assign proper quantum numbers to quasi-particle properties, identify excited states of quasi-particles, and calculate loop corrections to the classical results for observable quantities, which may be crucial for experimental verification. The evaluation of loop corrections necessarily brings about the need for renormalization. Although, generally effective field theories might be non–renormalizable in the strict sense, they still may be renormalized order by order in terms of a gradient expansion. A well-known example is chiral

perturbation theory (ChPT), applied successfully in hadron physics. In the vacuum sector such an expansion is truncated by allowing only for external momenta small compared to the underlying scale of the theory. However in the soliton sector, the soliton itself constitutes "external" fields with gradients comparable to the scale of the theory which cannot be made small by definition. Therefore, in dealing with solitons, the problem of truncating the expansion can only be solved by the ad hoc assumption that the renormalized couplings of the higher gradient terms are small.

A prominent example for the application of this program are 3D-$SU(N_f)$ skyrmions in N_f-flavor meson fields, where the topological charge is identified with baryon number, with impressive success for baryonic properties, resonances, and meson-baryon dynamics. Similarly, the conjecture to consider 2D-$O(3)$ spin textures as charged quasi-particles in ferromagnetic quantum Hall systems [1] and antiferromagnetic high–temperature superconductors [2], with topological winding density identified with the deviation of the electron density from its uniform background value, suggests a corresponding investigation. For magnons and vortices with unity charge such attempts have been presented for ferromagnets [3] and antiferromagnets [4]. The field theoretical approach forwarded here is rather related to the antiferromagnet due to its preserved time–reversal invariance which makes the analysis fairly similar to what applies to relativistic systems. The ferromagnet where time–reversal invariance is broken would require the consideration of the Landau–Lifshitz dynamics. The evaluation of the Casimir energies involves bound–state energies and a sum over scattering phase–shifts [5]. This provides also complete information about resonant excited states in the continuum which in the 3D-$SU(N_f)$ case successfully describe well-established baryon resonances.

For the general outline of the necessary steps and technique we discuss the case where the second-order exchange energy is taken in the time–reversal invariant form of the non–linear sigma model as it naturally appears in relativistic field theories. In two dimensions it is scale invariant and therefore irrelevant for the spatial extent of the static localized solution. To fix the soliton size two more terms are needed. We use the standard fourth-order Skyrme term, and a symmetry-breaking coupling of the $O(3)$-order parameter to an anisotropy field. The static part of the Skyrme term represents a local approximation to the Coulomb energy of the charged excitations; in our field-theoretic example we keep also the time-derivative parts of it. So our discussion will mainly serve a demonstrative purpose as a model field theory.

We shall specifically address the question of the binding energy of doubly charged quasi particles. For 3D-$SU(N_f)$ skyrmions this question has a long history since it was discovered that in the winding number $B = 2$ sector the static lowest-energy solution is bound with respect to decay into two separate $B = 1$ skyrmions and displays only axial symmetry in contrast to the radially symmetric hedgehog skyrmions. There has been much discussion about the physical relevance (in the deuteron) of such a torus configuration, and it was speculated that quantum corrections might

reverse the sign of the binding energy $E(B=2)-2E(B=1)$. Evaluation of loop corrections to the 3D-$SU(2)$ $B=2$ torus is a formidable task which to our knowledge has not yet been achieved. It is interesting that the same situation occurs for the 2D-$O(3)$ skyrmions: the classical $n=2$ solution shows a ring-like density distribution and it is bound with respect to decay into two individual $B=1$ skyrmions. In this case, however, the evaluation of loop corrections for both configurations is of comparable complexity, and we will show that they in fact reverse the sign of the binding energy.

Actually, there is an ongoing discussion [6, 7] about the binding of 2-skyrmions also in condensed matter applications. However, it should be stressed that for ferromagnetic systems the time-dependent part of the effective lagrangian has to be replaced by the T-violating Landau-Lifshitz form with only one time derivative. For antiferromagnets the time derivative coupling of the staggered spin to the magnetic field, which does not contribute to the static stabilization should be included [8, 9, 10]. And, in any case, for quantitative conclusions, the non–local character of the Coulomb energy should be respected [11].

2 Static solutions

The Lagrangian of the $O(3)$ model in $2+1$ dimensions is conveniently written in terms of the 3-component field $\mathbf{\Phi}$ satisfying the constraint $\mathbf{\Phi}\cdot\mathbf{\Phi}=1$,

$$\mathcal{L}=\frac{f^2}{2}\partial_\mu\mathbf{\Phi}\partial^\mu\mathbf{\Phi}-\frac{1}{4e^2}(\partial_\mu\mathbf{\Phi}\times\partial_\nu\mathbf{\Phi})^2-f^2m^2(1-\Phi_3)\,. \tag{1}$$

The three terms represent the non–linear sigma (N$\ell\sigma$) model, the Skyrme and the potential term. There exists a conserved topological current

$$T^\mu=\frac{1}{8\pi}\epsilon^{\mu\nu\rho}\mathbf{\Phi}(\partial_\nu\mathbf{\Phi}\times\partial_\rho\mathbf{\Phi})\,,\qquad \partial_\mu T^\mu=0\,. \tag{2}$$

The radially symmetric hedgehog ansatz, written in polar coordinates (r,φ)

$$\mathbf{\Phi}=\begin{pmatrix}\sin F(r)\cos n\varphi\\ \sin F(r)\sin n\varphi\\ \cos F(r)\end{pmatrix}\,, \tag{3}$$

corresponds to winding number

$$\int d^2rT^0=\frac{n}{2}[\cos F(\infty)-\cos F(0)]=n\,,\qquad T^0=-\frac{nF'\sin F}{4\pi r} \tag{4}$$

and the soliton's size may be defined according to

$$<r^2>_n=\frac{1}{n}\int d^2r\,r^2T^0=-\frac{1}{4\pi}\int d^2r\,rF'\sin F\,. \tag{5}$$

It is convenient to absorb the length $1/\sqrt{fem}$ which sets the scale for the size of localized structures into the dimensionless spatial coordinate $x = \sqrt{fem}\, r$. The static energy functional connected with the lagrangian (1) is then given by

$$E_n^{class} = \frac{f^2}{2} \int d^2x \left[F'^2 + \frac{n^2 s^2}{x^2} + a\frac{n^2 F'^2 s^2}{x^2} + 2a(1-c) \right] = 4\pi f^2 E_n^0(a)\,, \qquad (6)$$

with the abbreviations $s = \sin F$ and $c = \cos F$. Technically, $a = m/fe$ is the only nontrivial parameter, while $4\pi f^2$ sets the overall energy scale. We shall therefore present results for different values of a. The limit $a \to 0$ describes the pure Belavin–Polyakov (BP) solution [12]. The opposite limit, $a \to \infty$, is technically also well defined; it describes a system without spin-spin aligning force.

The Euler–Lagrange equation following from the variation of the energy functional

$$\frac{1}{x}\,(xF')' - \frac{n^2 sc}{x^2} + a\frac{n^2 s}{x}\left(\frac{F's}{x}\right)' - as = 0 \qquad (7)$$

is a second order non–linear differential equation which is solved subject to the boundary conditions

$$F(0) = \pi\,, \qquad F(x \to \infty) = 0\,. \qquad (8)$$

In principle the boundary condition at the origin according to (4) could be $F(0) = \nu\pi$ with $\nu = 1, 3, \ldots$ an odd multiple of π, however it turns out that the solution with $\nu = 1$ has the smallest static energy.

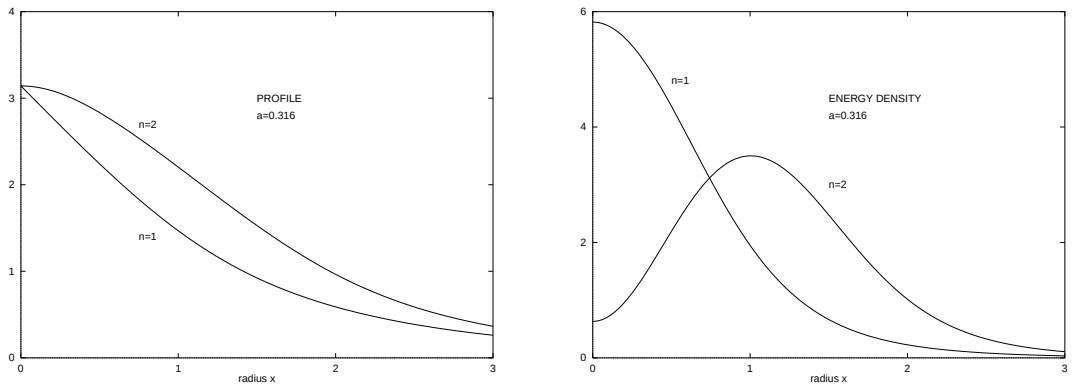

Figure 1: Hedgehog profiles and energy densities for the skyrmions with $n = 1$ and $n = 2$. The parameter $a^2 = 0.1$ was used.

The hedgehog profiles and the corresponding energy densities for $a^2 = 0.1$ are shown in Fig. 1 for the 1- and 2-skyrmions. It is noticed that the maximum energy

Table 1: Classical soliton energies and square radii for the stable 1- and 2-skyrmions for various parameters a.

a	0.0	0.01	0.0316	0.1	0.316	1.0
E_1^0	1.00	1.03	1.08	1.21	1.56	2.57
E_2^0	2.00	2.03	2.10	2.30	2.94	4.85
$< x^2 >_1$	∞	2.44	2.11	1.80	1.57	1.42
$< x^2 >_2$	π	3.11	3.06	2.99	2.78	2.76

density for the $n = 2$ soliton is not located at the origin but in a spherical shell of radius $x \simeq 1$.

The classical energies and square radii are given in Table 1. In the two limiting cases, $a \to 0$ and $a \to \infty$, the differential equation (7) may be solved analytically (see appendix). The corresponding static energies and radii are

$$\begin{aligned} E_n^0 &= n\,, & < x^2 >_n &= \sqrt{\tfrac{2n}{3}(n^2-1)} \cdot \tfrac{\pi/n}{\sin(\pi/n)} & a << 1 \\ E_n^0 &= 4n/3 \cdot a\,, & < x^2 >_n &= 4n/3 & a >> 1\,. \end{aligned} \quad (9)$$

It is noticed that for the BP solution with $a \to 0$ the 1-skyrmion's radius diverges which is due to the particular choice of the potential term in (1). This divergence is perceptible only for extremely small values of a, for $a \gtrsim 0.001$ the radius for the 1-soliton is still smaller than that of the 2-soliton which stays finite in the limit $a \to 0$ (for a more thorough discussion of this problem we refer to the appendix). The dependence of the energies on the dimensionless parameter a is shown in Fig. 2. Independently from this parameter $E_2^0 \leq 2E_1^0$ always holds, the 2-skyrmion is classically stable against decay into two 1-skyrmions. Hedgehog solutions with higher topological charge, $n \geq 3$, are not stable (see subsection 3.3 for their stability) and do not represent the minimum energy configuration of the corresponding sector. The 3-soliton's minimum energy configuration is not rotationally symmetric, it is a linear molecule which consists of three distorted 1-solitons. Higher multi–solitons are then supposedly molecules of stable 2-skyrmions (and 1-skyrmions in case of n odd) [13]. This picture may change fundamentally when the Casimir energies are taken into account.

3 Small amplitude fluctuations

The evaluation of quantum corrections is based on the normal modes of the classical configurations. With the appropriate boundary conditions these normal modes describe excited localized (bound) states, and the scattering of the vacuum fluctuations

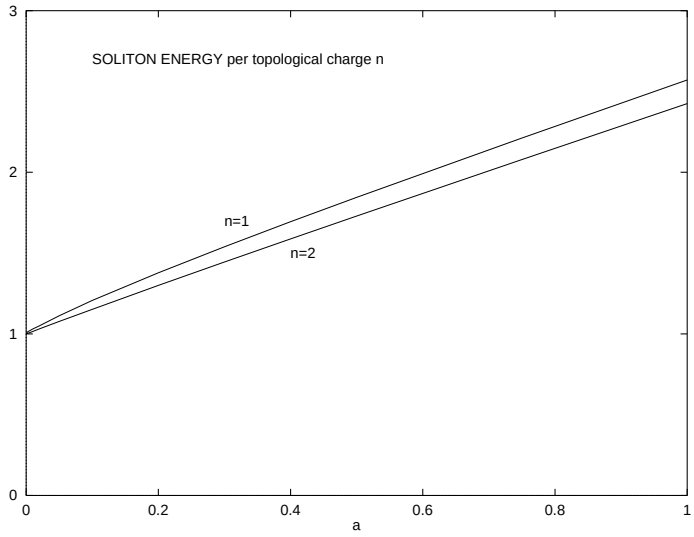

Figure 2: Classical soliton energies for $n = 1$ and $n = 2$ as functions of the dimensionless parameter a. For better comparison the energies plotted are divided by the corresponding topological charge. The 2-skyrmion is classically stable against decay into two 1-skyrmions.

(mesons or magnons) off the soliton backgound. (The S-matrix for magnon-vortex scattering has been considered (without the stabilizing Skyrme and potential terms) in [14] for antiferromagnets and in [15] for ferromagnets). Because of the constraint $\mathbf{\Phi} \cdot \mathbf{\Phi} = 1$ the model effectively possesses two independent fields. We therefore introduce two–component small amplitude fluctuations

$$\boldsymbol{\eta} = \hat{\boldsymbol{r}}_n \eta_L + \hat{\boldsymbol{\varphi}}_n \eta_T \,, \qquad \hat{\boldsymbol{r}}_n = \begin{pmatrix} \cos n\varphi \\ \sin n\varphi \end{pmatrix} \,, \quad \hat{\boldsymbol{\varphi}}_n = \begin{pmatrix} -\sin n\varphi \\ \cos n\varphi \end{pmatrix} \tag{10}$$

which we decompose into components parallel and perpendicular to the soliton configuration with winding number n. Of course, there are many different ways to parametrize the total time-dependent field $\mathbf{\Phi}$ which lead to different equations of motion for the corresponding fluctuations. However, the bound–states and the scattering matrix, in particular the phase–shifts are independent of the chosen parametrization. A very convenient choice different from the common Polyakov parametrization [16], which only at first sight may seem complicated, is given by

$$\mathbf{\Phi} = \begin{pmatrix} \hat{\boldsymbol{r}}_n \sin F(1 - \boldsymbol{\eta}^2/2) + \hat{\boldsymbol{r}}_n \cos F\eta_L + \hat{\boldsymbol{\varphi}}_n \eta_T \\ \cos F(1 - \boldsymbol{\eta}^2/2) - \sin F\eta_L \end{pmatrix} \stackrel{r\longrightarrow\infty}{\longrightarrow} \begin{pmatrix} \boldsymbol{\eta} \\ 1 - \boldsymbol{\eta}^2/2 \end{pmatrix} . \tag{11}$$

The main advantage of this parametrization is that it leads to a flat metric for the non–linear sigma model part of the lagrangian. For 3D-$SU(N)$ skyrmions this parametrization is well–known as Callan–Klebanov ansatz [17].

It is now straightforward to write down the e.o.m. for the fluctuating components η_L and η_T. The Lagrangian (1) has to be expanded to quadratic order in the fluctuations, then the e.o.m. can be read off. We give these coupled linear differential equations explicitely, where we have already exploited the time–dependence as well as the angular dependence of the fluctuations

$$\eta_L = \sum_M f_M(x) e^{iM\varphi} e^{-i\omega t}\,, \qquad \eta_T = i \sum_M g_M(x) e^{iM\varphi} e^{-i\omega t}\,. \tag{12}$$

The e.o.m. decouple in the magnetic quantum number M, which is the analogon of the phonon- (or grand-) spin familiar from scattering calculations for 3D-$SU(N)$ skyrmions

$$\begin{aligned}
&-\frac{1}{x}\left(x b_L f_M'\right)' + \frac{M^2}{x^2} f_M + \frac{n^2}{x^2}(b_T - 2s^2) f_M - a\frac{2n^2 c}{x}\left(\frac{F's}{x}\right)' f_M + acf_M \\
&\qquad -\frac{nMc}{x^2}(1+b_T) g_M + a\frac{nMF's}{x^2} g_M' + a\frac{2nM}{x}\left(\frac{F's}{x}\right)' g_M = \omega^2 b_L f_M \\
&-\frac{1}{x}\left(x g_M'\right)' + \frac{M^2}{x^2} b_T g_M - (F'^2 - \frac{n^2 c^2}{x^2}) g_M - a\frac{n^2 c}{x}\left(\frac{F's}{x}\right)' g_M + acg_M \\
&\qquad -\frac{nMc}{x^2}(1+b_T) f_M - a\frac{nMF's}{x^2} f_M' + a\frac{nM}{x}\left(\frac{F's}{x}\right)' f_M = \omega^2 b_T g_M\,.
\end{aligned} \tag{13}$$

Here we introduced the metric functions $b_L(x) = 1 + an^2 s^2/x^2$ and $b_T(x) = 1 + aF'^2$. The energies ω are understood in natural units of $\sqrt{fem}$ such that the threshold occurs at $\omega = \sqrt{a}$. The equations are invariant with respect to the simultaneous replacements $M \to -M$ and $g_M \to -g_M$. These equations contain all the information about zero–modes, bound–states, the scattering matrix and the stability of the hedgehog solutions.

3.1 Zero-modes

The soliton's energy (6) is invariant under spatial rotations around the z-axis (which for the hedgehog is equivalent to an iso–rotation around the internal 3-axis) as well as under a translation in the x-y plane. The infinitesimal rotation (iso–rotation) and translation give rise to zero–modes which are solutions of the e.o.m. (13) for $\omega^2 = 0$.

The rotational zero–mode is obtained by a shift of the azimuthal angle $\varphi \to \varphi + \alpha$ in the hedgehog ansatz (3). Comparison with (11) and (12) shows then that this zero–mode

$$f_0(x) = 0\,, \quad g_0(x) = s \qquad \text{(rotational zero-mode)} \tag{14}$$

is located in the $M = 0$ partial–wave. Similarly, the translational zero–mode $\boldsymbol{r} \to \boldsymbol{r} + \boldsymbol{a}$

$$f_1(x) = F' \,, \quad g_1(x) = \frac{ns}{x} \qquad \text{(translational zero-mode)} \tag{15}$$

sits in the $M = 1$ partial–wave.

With the stability condition (7) it is easily checked that the above modes satisfy the e.o.m. for $\omega^2 = 0$. As both zero–modes possess a finite norm, they will act as bound–states in the scattering calculation and influence the phase–shifts via Levinson's theorem. Besides these zero energy bound–states there are also bound–states at finite energy.

3.2 Bound-states

In both systems, $n = 1$ and $n = 2$, we observe bound–states in the $M = n$ partial–wave. With decreasing parameter a the energies of these bound–states move towards the threshold, in particular for the $n = 1$ system this happens very quickly (cf. Table 2). There is a simple explanation of this phenomenon. As is noticed from the e.o.m. the iso–rotation with respect to the 1- and 2-axes

$$f_n(x) = 1 \,, \quad g_n(x) = c \qquad \text{(zero-energy solution for} \quad a \to 0) \tag{16}$$

is a zero–energy solution of the $M = n$ partial–wave for $a \to 0$. The potential connected with a finite $a \neq 0$ distorts this continuum solution into a bound–state, which in the limit $a \to 0$ is shifted towards the threshold.

Table 2: Bound-state energies relative to the threshold in the $M = n$ partial–wave. With decreasing parameter a the bound–states move towards threshold.

a	1.0	0.707	0.316	0.224	0.1	0.071
$n = 1$	0.943	0.99994	$\simeq 1.0$	$\simeq 1.0$	$\simeq 1.0$	$\simeq 1.0$
$n = 2$	0.330	0.394	0.622	0.690	0.866	0.943

In the $n = 1$ system this is the only bound–state apart from the zero–modes already discussed. However in the $n = 2$ case some of the low-lying resonances may also become bound for sufficiently strong a, e.g. for $a = 1$ we find additional bound–states in the $M = 0$ and $M = 1$ partial–waves at energies $\omega_0 = 0.923$ and $\omega_1 = 0.793$ respectively. All these bound–states must be considered for the Casimir energy (compare also the discussion of the phase–shifts in subsection 3.4).

3.3 Stability of hedgehog solitons

Formally, eqs. (13) are the e.o.m. for small amplitude fluctuations around a hedgehog soliton with arbitrary topological quantum number n. For this reason they contain information about the stability of the n-skyrmion. For the n-skyrmion to be stable there must not exist solutions to (13) with negative ω^2.

Indeed, we do find solutions of (13) with negative ω^2 for topological quantum numbers $n \geq 3$. For example for $n = 3$ with $a^2 = 0.1$ there exist such solutions in the $M = 2$ ($\omega^2 = -0.14$), $M = 3$ ($\omega^2 = -0.30$) and all higher partial waves. In the $n = 1$ and $n = 2$ sectors there exist no negative ω^2 solutions.

We conclude, that the $n = 1$ and $n = 2$ hedgehog solitons are stable while those with higher topological charges are unstable. This agrees with the findings in ref. [13]. In what follows we consider the scattering off the stable skyrmions with $n = 1$ and $n = 2$.

3.4 Phase–shifts

For the 2-dimensional scattering problem in spherical coordinates [18] the incident plane wave is decomposed into partial waves carrying magnetic quantum numbers

$$e^{i\boldsymbol{pr}} = \sum_{M=-\infty}^{\infty} i^M J_M(pr) e^{iM\varphi} = \sum_{M=0}^{\infty} \epsilon_M i^M J_M(pr) \cos(M\varphi)\,. \tag{17}$$

The latter transformation with the multiplicities $\epsilon_0 = 1$ and $\epsilon_M = 2$ for $M \geq 1$ follows from the properties of the regular and irregular Bessel functions of the first kind, $J_M(pr)$ and $N_M(pr)$, when $M \to -M$. Thus, it suffices to consider the partial waves $M \geq 0$. Similarly, for the scattered wave (plane wave plus outgoing radial wave) in the case of a single channel we have

$$\Psi \;=\; \sum_{M=0}^{\infty} \epsilon_M i^M \psi_M(p,r) \cos(M\varphi)\,. \tag{18}$$

The partial–wave projected scattering waves $\psi_M(p,r)$ with appropriate boundary conditions at the origin are integrated according to the e.o.m. and the phase–shifts then are obtained from the asymptotic form

$$\psi_M(p,r) \to [J_M(pr)\cos\delta_M(p) + N_M(pr)\sin\delta_M(p)] e^{i\delta_M(p)}\,. \tag{19}$$

The phase–shifts are related to the cross–section in the usual way, and the property $\delta_M(p) = \delta_{-M}(p)$ follows from the corresponding symmetry of the e.o.m.. The generalization to two coupled channels now is straightforward. It is noticed that our scattering equations (13) decouple asymptotically when the functions $f_\pm = (f_M \mp g_M)/\sqrt{2}$ are introduced

$$-\frac{1}{r}\left(r f_\pm'\right)' + \frac{(M \pm n)^2}{r^2} f_\pm = p^2 f_\pm\,, \qquad \omega^2 = p^2 + m^2\,, \tag{20}$$

with the solution

$$f_\pm(p,r) = A_\pm(p) J_{|M\pm n|}(pr) + B_\pm(p) N_{|M\pm n|}(pr)\,. \tag{21}$$

From the coefficients $A_\pm(p)$ and $B_\pm(p)$ of the asymptotical solution, the 2×2 scattering matrix S_M is obtained for every partial wave M. Again, as the e.o.m. are invariant with respect to $M \to -M$ so is the scattering matrix and it suffices to consider $M \geq 0$. It is convenient to diagonalize the scattering matrix

$$S_M = U_M \begin{pmatrix} e^{i\delta_M^{(1)}} & 0 \\ 0 & e^{i\delta_M^{(2)}} \end{pmatrix} (U_M)^\dagger\,, \tag{22}$$

in order to obtain the intrinsic eigen phase–shifts $\delta_M^{(1)}$ and $\delta_M^{(2)}$. Their sum $\delta_M = \delta_M^{(1)} + \delta_M^{(2)}$ is plotted for the partial waves with $M \leq 4$ in Fig. 3, where the $n=1$ and $n=2$ systems are considered separately.

The picture that emerges looks qualitatively quite similar to what has been obtained for 3D-$SU(N)$ skyrmions long ago [19]. For topological charge $n=1$ we obtain in detail: The phases for $M=0$ and $M=1$, where the rotational and translational zero modes are located together with the $M=1$ bound–state, start at π resp. 2π according to Levinson's theorem. For the smaller parameters $a^2 = 0.01$ and 0.1 the wave–function of the $M=1$ bound–state close to threshold (Table 2) is already quite similar to the infinitesimal translation (cf. subsection 3.5 for the limit $a \to 0$). As a consequence the phase–shift at threshold reacts with a sudden drop from 2π to π which in the figures is only noticed because the phase–shift falls below π before it bends to the right. A weakly pronounced breathing mode is observed at low energies for $M=0$. The partial–waves $M=2,3,\ldots$ then contain a band of resonances which are flattened out for higher M and also with decreasing parameter a.

Similarly for topological charge $n=2$: For the smaller parameters $a^2 = 0.01$ and 0.1 the $M=0$ and $M=1$ phase–shifts start at π because of the zero modes. In all but the $M=2$ partial–wave with its bound–state (cf. Table 2) sharp resonances occur, which are much more pronounced compared to the $n=1$ case. For strong potentials then, the $M=0$ and $M=1$ resonances become bound (e.g. for $a=1$ at $\omega_0 = 0.923$ and $\omega_1 = 0.793$). Also less pronounced secondary resonances do appear.

3.5 Belavin-Polyakov soliton

Finally we would like to add a few comments on the pure Belavin–Polyakov solution [12]. As mentioned we recover this solution for small parameters a with its size R still fixed by the balance of the Skyrme and potential terms (cf. appendix). In the pure N$\ell\sigma$ model without additional stabilizing terms the size R of the BP

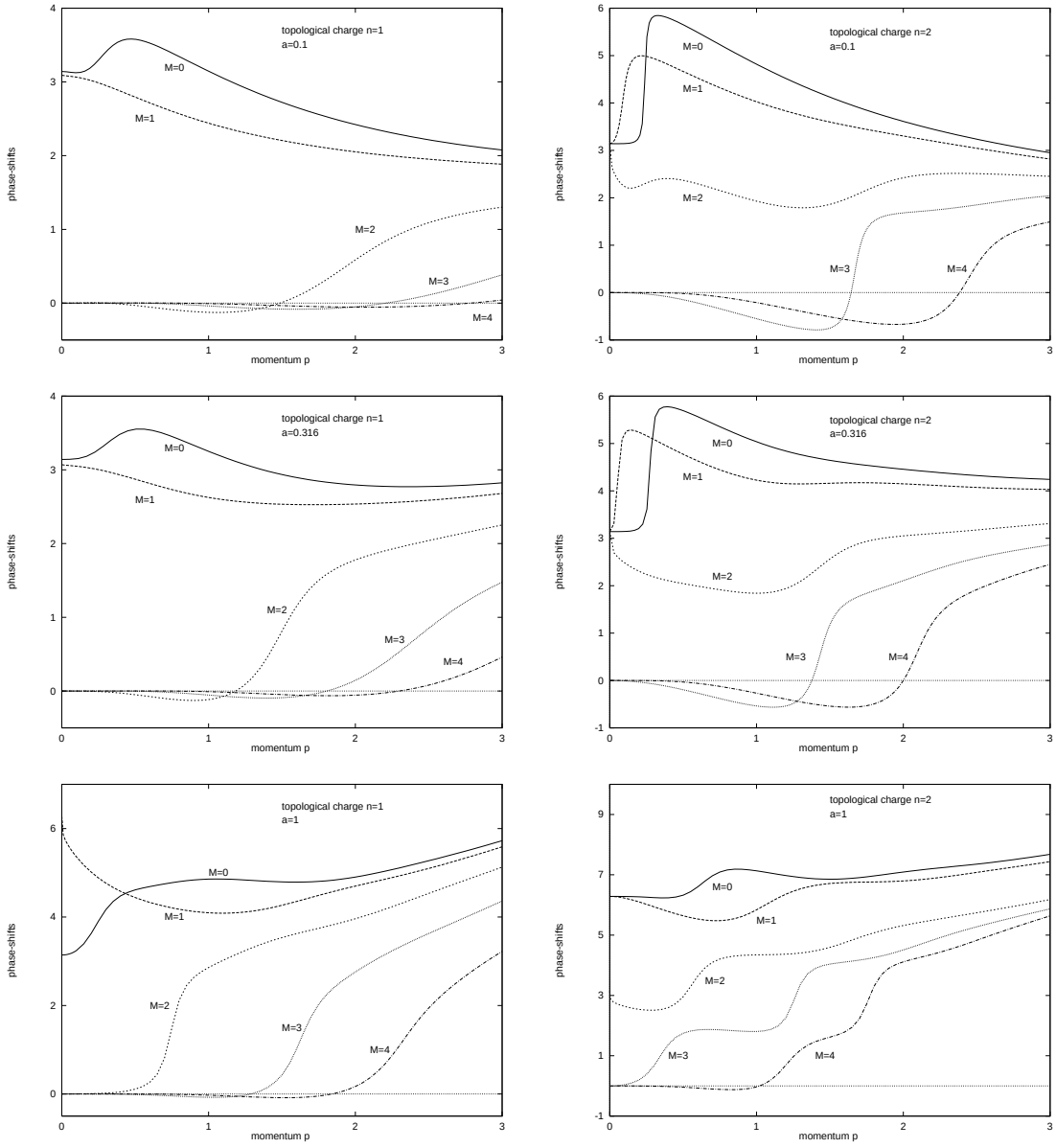

Figure 3: Phase shifts for the lowest partial waves scattered off the stable $n = 1$ and $n = 2$ skyrmions. The relevant parameter was fixed at $a^2 = 0.01$, 0.1 and 1.0. The momentum p is plotted in natural units. According to Levinson's theorem the phase–shifts start at multiples of π. Many resonances are observed in the various channels.

soliton is an undetermined parameter. In contrast to the full lagrangian (1) the pure N$\ell\sigma$ model does not break $O(3)$–symmetry and is also conformally invariant. Due to these additional symmetries a larger number of zero–modes is expected.

The e.o.m. for the fluctuations obtained in that case from (13) with $a = 0$ and $x = r/R$ decouple for $f_\pm = (f_M \mp g_M)/\sqrt{2}$ (not only asymptotically) and are easily solved. Still the counting of the zero–modes is a bit tricky. In addition to the rotation (14), the breathing–mode (conformal invariance) becomes a zero–mode in the $M = 0$ partial–wave as expected. But for the 1–soliton the iso–rotation (16) coincides with the translation (15) giving rise to only 2×1 zero–modes in the $M = 1$ partial–wave. This makes altogether 4 zero–modes for the 1–soliton. Similar counting for the 2–soliton yields 8 zero–modes.

Of course, this discussion is somewhat academic, because in reality there should always be some stabilizing term which fixes the size of the soliton and which at least breaks conformal invariance. Therefore we do not show the corresponding phase–shifts.

4 Casimir energy

With the bound–state energies and the phase–shifts provided in the previous section we are in the position to evaluate the 1-loop contribution to the soliton energy, i.e. the Casimir energy. The UV singularities contained in the loop are related to the high momentum behaviour of the phase–shifts

$$\delta(p) = \sum_{M=0}^{\infty} \epsilon_M \delta_M(p) \stackrel{p\longrightarrow\infty}{\longrightarrow} a_0 p^2 + a_1 \,. \tag{23}$$

In the case of a vanishing Skyrme term the coefficients

$$a_0 = 0\,, \qquad a_1 = \frac{1}{4}\int d^2r \left[F'^2 + \frac{n^2 s^2}{r^2} + 2m^2(1-c)\right] \tag{24}$$

are known analytically from the Born terms. For the full model they have to be extracted numerically from the phase–shift sum (23), which for that purpose has to be calculated to a high precision with some 100 partial waves taken into account. Typical values obtained, e.g. for $a^2 = 0.1$, are $a_0 = 1.0(fem)^{-1}$ and $a_1 = 7.2$ for the 1-soliton, and $a_0 = 2.0(fem)^{-1}$ and $a_1 = 13.4$ for the 2-soliton respectively. According to (24) the N$\ell\sigma$ plus potential term contributions to these coefficients are $a_1 = 8.3$ for $n = 1$ and $a_1 = 15.6$ for $n = 2$. With this established we may use the phase–shift formula [5], subtract the troublesome high momentum behaviour from the phase–shifts, and separately add the corresponding counterterms

$$E^{1-loop} \;=\; \frac{1}{2\pi}\left[-\int_0^\infty dp \frac{p}{\omega}\delta(p) - m\delta(0)\right] + \frac{1}{2}\sum_B \omega_B \tag{25}$$

$$= -\frac{1}{2\pi}\int_0^\infty dp\frac{p}{\omega}\left(\delta(p)-a_0p^2-a_1\right)+\frac{1}{2}\sum_B(\omega_B-m)-\int\frac{d^2p}{(2\pi)^2}\,\frac{a_0p^2+a_1}{\omega}\,.$$

This procedure is closely related to what has been employed in the $3+1$ dimensional Skyrme model for the calculation of the Casimir energy to the nucleon mass [20, 21]. The counter terms could e.g. be evaluated using a 2-momentum cutoff $\Lambda >> m$

$$\int\frac{d^2p}{(2\pi)^2}\,\frac{1}{\omega}=\frac{1}{2\pi}[\Lambda-m]\,,\qquad\int\frac{d^2p}{(2\pi)^2}\,\frac{p^2}{\omega}=\frac{1}{6\pi}[\Lambda^3-\frac{3}{2}m^2\Lambda+2m^3]\,,\tag{26}$$

which makes the linear and cubic divergencies explicit

$$E^{1-loop}=-\frac{a_0}{6\pi}\left[\Lambda^3-\frac{3}{2}m^2\Lambda\right]-\frac{a_1}{2\pi}\Lambda+E^{cas}\,.\tag{27}$$

While the N$\ell\sigma$ and the potential term contributions located in a_1 may be absorbed in a renormalized constant

$$f^2=\bar{f}^2-\frac{\Lambda}{4\pi}\tag{28}$$

($\bar{f}$ denotes the bare constant), the divergencies stemming from the Skyrme term renormalize the Skyrme parameter e as well as the couplings of all the higher gradient terms not listed in the lagrangian (1). The latter renormalization we do not carry out explicitely, instead we simply assume that the renormalized Skyrme parameter be e and the renormalized couplings of the higher gradient terms be zero. To which extent this is a consistent assumption will be discussed in the following section in connection with the scale–dependence of our results. Now all the divergencies residing in (27) are taken care of, leaving the finite Casimir energy

$$E^{cas}=-\frac{1}{2\pi}\int_0^\infty dp\frac{p}{\omega}\left(\delta(p)-a_0p^2-a_1\right)+\frac{1}{2}\sum_B(\omega_B-m)-\frac{a_0m^3}{3\pi}+\frac{a_1m}{2\pi}\,.\tag{29}$$

This result is independent of the employed regularization scheme. For instance, using dimensional regularization the counter terms (26) in $2+1$ dimensions become finite and equal to the last terms in the brackets, respectively, which yields the same expression for the Casimir energy. However, although dimensional regularization in odd dimensions has been used right from the beginning [22] and is now commonly applied in Φ_3^4, QCD$_3$ and Chern-Simons theories [23, 24], we hesitate to apply this scheme for an odd number of dimensions because the fate of the UV singularities remains obscure. As the divergencies do not show up in odd dimensional regularization there seems to be no possibility to introduce a renormalization scale. For strictly (super) renormalizable theories this may be of no further importance, however in theories which are renormalized order by order in terms of a gradient expansion a scale is desirable in order to control the convergence of the series (cf. section 5).

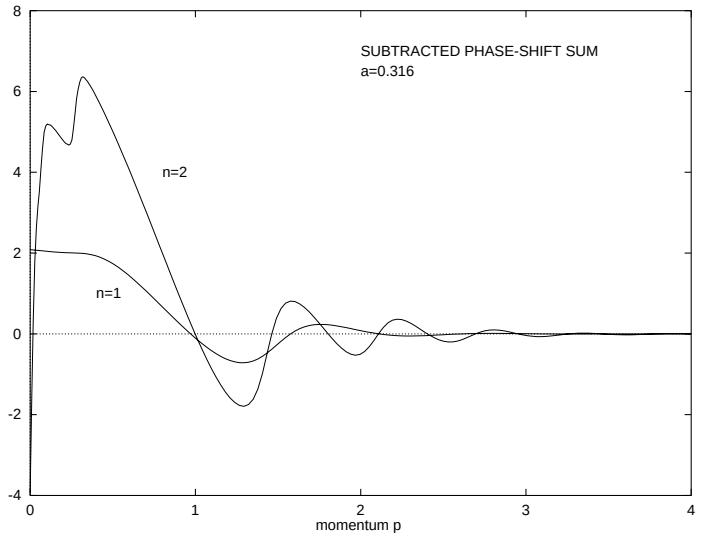

Figure 4: Subtracted phase–shift sum as a function of the momentum p in natural units for the $n = 1$ and $n = 2$ systems calculated with $a^2 = 0.1$.

The Casimir energy (29) consists of three parts, i.e. the phase–shift integral, the bound–state contribution and the contribution from the counter–terms.

The subtracted phase–shift sum $\delta(p) - a_0 p^2 - a_1$ which enters the phase–shift integral is plotted in Fig. 4 for the $n = 1$ and $n = 2$ systems ($a^2 = 0.1$). The maximum momentum to which this sum has to be integrated depends sensitively on the parameter a. The various contributions to the Casimir energy are given in Table 3 for several values of a. The dependence of the Casimir energies on

Table 3: Individual contributions to the Casimir energy according to (29) for the $n = 1$ and $n = 2$ systems. All energies are given in natural units.

	$n=1$			$n=2$		
a	0.1	0.316	1.0	0.1	0.316	1.0
phase-shifts	−0.29	−0.08	0.00	−0.63	−0.26	0.05
bound-states	−0.47	−0.84	−1.56	0.52	−1.06	−2.47
counter terms	0.31	0.62	1.85	0.61	1.16	3.36
total	−0.45	−0.30	0.29	−0.54	−0.15	1.00

this parameter is shown in Fig. 5. Note that for an easier comparison again only half of the 2-skyrmion's Casimir energy is plotted. It is noticed that the Casimir energy of the 1-skyrmion stays always smaller compared to half of that of the 2-skyrmion. Therefore, in contrast to the classical energy the Casimir energy favors

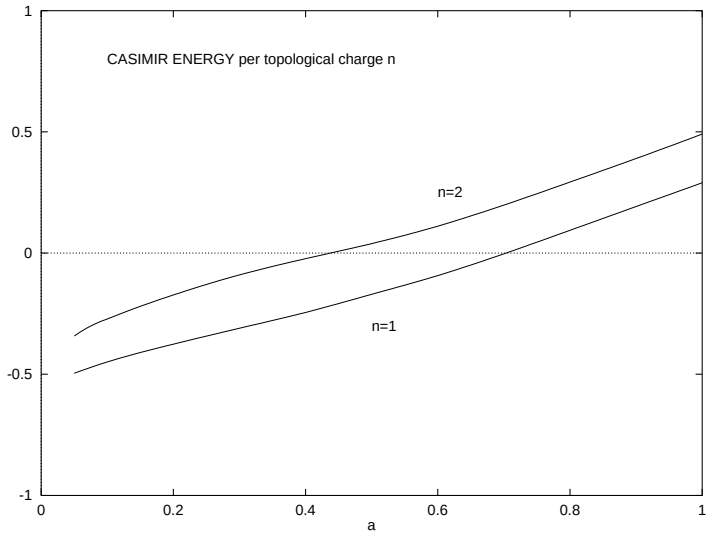

Figure 5: Casimir energies in natural units for the 1- and 2-skyrmion devided by their topological charge.

single skyrmions. These competing effects may be summarized in the formula for the total energy cast into the form

$$\begin{aligned} E_n^{total} &= 4\pi f^2 E_n^0(a) + \sqrt{fem} E_n^1(a) \\ &= 4\pi f^2 \left[E_n^0(a) + y\, E_n^1(a) \right] , \qquad\qquad y = \frac{\sqrt{fem}}{4\pi f^2} , \end{aligned} \tag{30}$$

where $E_n^1(a)$ represents the Casimir energy (29) in natural units $\sqrt{fem}$. Thus, apart from the overall scale $4\pi f^2$ the model is characterized by the two dimensionless parameters a and y. If this ratio y exceeds a critical value (which increases slowly with a, e.g. $y = 0.3, 0.4, 0.7$ for $a^2 = 0.01, 0.1, 1.0$), then $E_2^{total} - 2E_1^{total}$ becomes positive and the 2-skyrmion decays into two single 1–skyrmions.

4.1 Numerical example from hadron physics

Although different dimensionalities may cause qualitative differences, let us illustrate these results by a numerical example using the scale of hadron physics: Take the value $a = 0.1$, fix the size scale at $1/\sqrt{fem} = 0.2fm$ ($\sqrt{fem} = 1$ GeV) and make use of the numbers given in Table 1 and Table 3. With the above parameters the 1-soliton gets a topological radius 0.27 fm and a Casimir energy $E_1^{cas} = -0.45$GeV, a situation very similar to what has been obtained in the hadronic Skyrme model [21], if in addition the classical soliton mass is fixed at $E_1^{class} = 1.21(4\pi f^2) = 1.39$ GeV in order to obtain the nucleon mass at $E_1^{total} = 0.94$ GeV. Then the $n = 2$ soliton's total energy $E_2^{total} = (2.64 - 0.53)$ GeV $= 2.11$ GeV turns out to be larger than

that of two separated 1-skyrmions. The parameter in this example, $y = 0.9$, lies far above the critical value 0.3. Of course, the $2+1$ dimensional model discussed here cannot be taken literally for hadron physics, but exactly this mechanism may shift the undesired torus configuration obtained in hadronic soliton models with baryon number $B = 2$ to higher energies.

4.2 Casimir energy of the pure Belavin-Polyakov soliton

Finally we would like to discuss the Casimir energy of the pure BP soliton with free size parameter R in order to make contact to the quantum corrections as obtained in ref. [4]. With $m = 0$ and the coefficients $a_0 = 0\,,\ a_1 = 2\pi n$ and no additional bound–states present (cf. the discussion about the zero–modes in subsection 3.5) eq.(25) for the 1–loop contribution simplifies

$$\begin{aligned} E^{1-loop} &\stackrel{BP}{=} -\frac{1}{2\pi}\int_0^{(\Lambda)} dp\delta(p) \\ &= -\frac{1}{2\pi}\int_0^{(\Lambda)} dp\,(\delta(p) - a_1) - \frac{a_1}{2\pi}\Lambda \\ &= -\frac{1}{2\pi R}\int_0^{(\Lambda R)} d(pR)\,(\delta(pR) - 2\pi n) - n\Lambda\,. \end{aligned} \tag{31}$$

We indicate here the possibility to limit the momentum integration by a finite Debye momentum $\Lambda = p_D$ related to the lattice constant. Because the soliton should at least cover several lattice sites, $\Lambda R > 1$ is large enough to extend the integration over the subtracted phase–shifts to infinity (see Fig. 4) just as in our field theoretical treatment. Through the substitution in the last step the dependence of the subtracted phase–shift integral on the soliton size R becomes explicit: the magnitude of the Casimir energy decreases with increasing soliton size.

Numerically, we find

$$E_1^{cas} = -\frac{0.5}{R_1}\,, \qquad\qquad E_2^{cas} = -\frac{1.7}{R_2} \tag{32}$$

for the pure BP solitons with topological charges $n = 1$ and $n = 2$ respectively. Their sizes R_1 and R_2 are arbitrary and generally different. If the sizes are determined by the stabilizing terms in the limit $a \to 0$, we obtain $R_n = b_n/\sqrt{fem}$ with $b_1 \to 0$ and $b_2 \to \sqrt{2}$ (appendix). For that reason the Casimir energy of the 1-soliton plotted in Fig. 5 bends to negative values and finally diverges as a approaches zero. The Casimir energy of the 2-soliton stays finite, $E_2^1 = -1.7/\sqrt{2} + \mathcal{O}(\sqrt{a})$, but with an infinite slope at $a = 0$.

In ref. [4] the subtracted phase–shift integral was neglected for $p_D R >> 1$ and the last term in (31) then lead to the result $E^{1-loop} \stackrel{BP}{=} -np_D$. Because this is exactly the term we absorb into a renormalized f^2 (27,28), this result corresponds to $E^{cas} = 0$

in our notation. The opposite limit $p_D R << 1$ where the 1-loop contribution (31) vanishes corresponds to soliton sizes much smaller than the lattice spacing and does not make sense. The conclusion, that the quantum corrections lower the soliton energy as soliton size increases, is wrong.

5 Scale dependence

In this section we introduce a scale μ which allows to shift finite pieces from the tree to the 1-loop contribution and vice versa. It will be introduced in such a way that we recover the results of the previous section for $\mu = \mu_0$. Tentatively, $\mu_0 = 4\pi f^2$ may be identified with the underlying energy scale of the model in analogy to the chiral scale $\mu_0 = 4\pi f_\pi \simeq 1\text{GeV}$ of ChPT [25]. Our results will however be presented in such a way that no fixation of μ_0 is required. For this purpose we write the cutoff characterizing the divergencies of the 1-loop contribution (27) as a sum of two parts $\Lambda = [\Lambda - (\mu - \mu_0)] + (\mu - \mu_0)$. The first part is then renormalized into a scale-dependent strength of the N$\ell\sigma$ and potential term

$$f^2(\mu) = \bar{f}^2 - \frac{\Lambda - (\mu - \mu_0)}{4\pi} = f^2 + \frac{\mu - \mu_0}{4\pi}\,. \tag{33}$$

According to this formula $\mu \neq \mu_0$ shifts the energy scale $4\pi f^2(\mu)$ away from its original value $4\pi f^2$. In order to exhibit the scale–dependence it is now convenient to present our results as function of the ratio $f^2(\mu)/f^2$ rather than μ itself. The presentation is then independent of μ_0 and also robust against changes in the regularisation scheme which may introduce numerical factors to the scale (e.g. in the 3-momentum instead of the 2-momentum cutoff scheme the scale is changed by a factor of $\pi/2$). The second part of the above decomposition, $(\mu - \mu_0)$, remains explicit in the finite Casimir energy

$$\begin{aligned} E^{cas}(\mu) &= -\frac{1}{2\pi}\int_0^\infty dp \frac{p}{\omega}\left(\delta(p) - a_0 p^2 - a_1\right) + \frac{1}{2}\sum_B(\omega_B - m) \\ &\quad + \frac{a_0}{6\pi}\left[(\mu-\mu_0)^3 - \frac{3m^2}{2}(\mu-\mu_0) - 2m^3\right] - \frac{a_1}{2\pi}\left[\mu - \mu_0 - m\right]\,. \end{aligned} \tag{34}$$

Also for the a_0 - term with its cubic divergence we kept all contributions from the second part in the Casimir energy although other prescriptions are possible. However this ambiguity will not influence the results strongly because of the smallness of a_0 (cf. numbers in the previous section). In this way both, the tree and the 1-loop contributions become scale–dependent. While for the N$\ell\sigma$ and potential terms the scale–dependence in the total soliton energy is exactly compensated, the 1-loop contribution which arises from the Skyrme term would not only yield a scale–dependent Skyrme parameter $e(\mu)$, but would also switch on all higher gradient

terms assumed to be zero for $\mu = \mu_0$. Having assumed all these couplings to be independent of the scale implies that the tree + 1-loop contribution to the soliton energy cannot be strictly scale–invariant. In fact, the resulting scale–dependence measures the magnitude of the higher gradient terms not accounted for. All the more it comes as a surprise, just as in the hadronic case [21], that for specific parameter choices an almost scale–independent soliton mass may be obtained. Such a case ($a^2 = 0.1, y = 1$) is depicted in Fig.6 for the 1-soliton. The rather strong scale–dependence of the tree contribution is nicely compensated over a wide range $f^2(\mu) = 0.5f^2, \ldots, 2.0f^2$ when the 1-loop contribution is added. Of course, this statement has to depend on the parameters used. Therefore in Fig. 7 we plotted the total 1-soliton mass for $a^2 = 0.1$ and various values of the ratio y. It is noticed that weak scale–dependence requires a ratio close to $y \simeq 1$, the value used in the previous figure. Lower and higher values of y enhance the scale–dependence. We do not show the corresponding plots for the 2-soliton because they look quite similar, with the scale–dependence being even somewhat weaker in that case.

We may now pose the question for which parameter combinations a and y we may expect a modest scale–dependence in accordance with the assumption that the couplings of all higher gradient terms are zero. The answer is illustrated in Fig.8. Inside the inner contour the average scale–dependence in the intervall $f^2(\mu)/f^2 \in [0.5, 2]$ is less than 3%. For comparison the 6% contour is also plotted.

All the parameter combinations lying inside the contours yield negative Casimir energies whose absolute values though sizeable do not exceed 50% of the classical soliton mass. They also lead to an unstable 2-soliton which decays into two individual 1-solitons. In particular the parameters ($a = 0.1, y = 0.9$) of our numerical example from hadron physics (section 4.1) lie in the center of the almost scale–independent region.

The weak scale dependence obtained for parameter combinations lying inside the contours in Fig. 8 implies that loop–corrections can be reliably calculated within the framework of the lagrangian (1) with all higher couplings set equal to zero.

6 Conclusions

We studied the magnon–vortex system in the $2+1$ dimensional $O(3)$ model in a field theoretical approach. For that purpose the N$\ell\sigma$ model was augmented by stabilizing standard fourth–order Skyrme and potential terms.

Complete information on bound and scattering states in all partial–waves was established. We find an extremely rich excitation spectrum with pronounced resonances as in the 3D-$SU(N_f)$ case with its baryon resonances. In principle these resonances should be accessible by measuring the excitation spectrum of spin–waves in the presence of skyrmions.

Furthermore, the quantum fluctuations will allow to study their influence on the

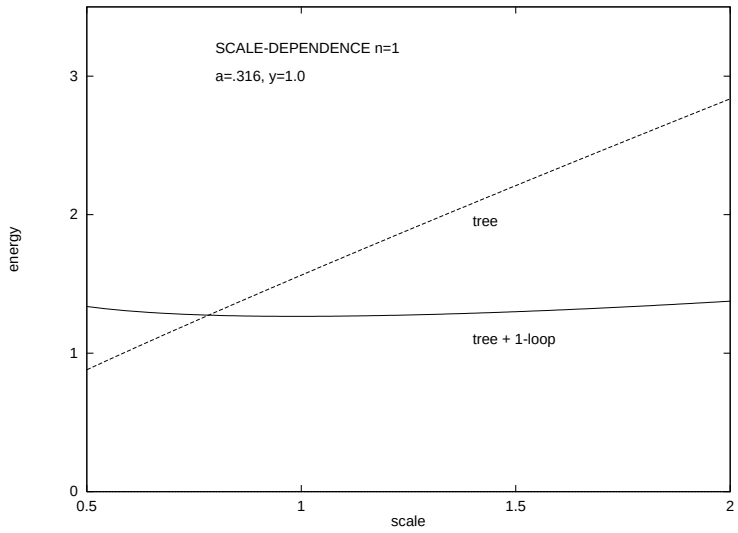

Figure 6: Scale-dependence of the 1-soliton's energy in tree and tree + 1-loop. The dimensionless parameters are $a = a(\mu_0) = .316$ and $y = y(\mu_0) = 1.0$. The energy is in units $4\pi f^2$ and the scale is given by the ratio $f^2(\mu)/f^2$.

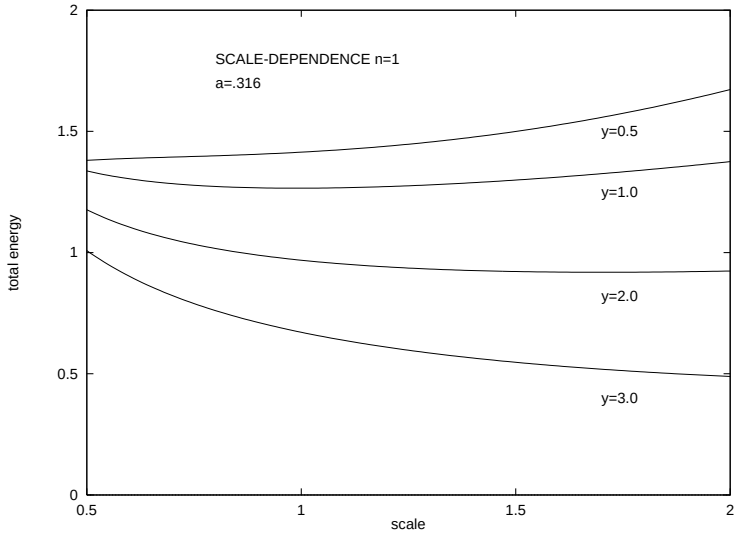

Figure 7: Scale-dependence of the 1-soliton's energy in tree + 1-loop for $a = a(\mu_0) = .316$ and various parameters $y = y(\mu_0)$. Energy and scale as in Fig. 6.

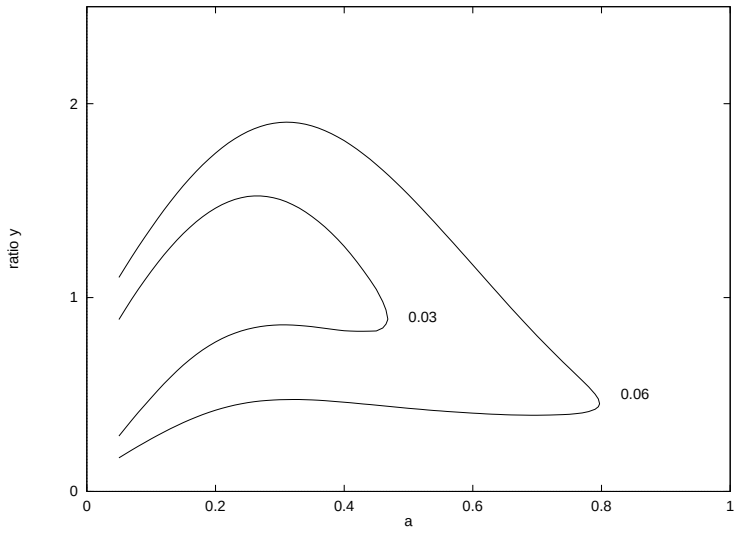

Figure 8: Parameter space (a, y) for 1-skyrmions. Inside the inner contour the scale–dependence is less than 3%, inside the outer contour less than 6%.

shape of the soliton [3]. Note that in tree approximation the third component of the order parameter field is always tied to -1 at the origin for topological reasons, in variance with microscopic Hartree-Fock calculations for the ferromagnet [26] which suggest a vanishing value in case of small solitons.

Finally with the bound state energies and the scattering phase–shifts the Casimir energies were evaluated. The appearing UV singularities were renormalized under the assumption that the (renormalized) couplings of the higher gradient terms be small. A criterium for the consistence of this assumption is the approximate scale–independence of the results such that the effective action represents an almost 1-loop renormalizable theory. This criterium requires a detailed balance of tree and 1-loop contributions which limits the parameter space where this requirement is met. The following results apply for this restricted parameter space. Parameters lying outside that range may lead to other conclusions, but there the 1-loop contribution cannot be reliably calculated within the model.

- The Casimir energy is negative and generally large leading to a considerable reduction of the total soliton energy. However, it does not exceed 50% of the tree contribution and thus may still be considered a (sizeable) correction.

- The magnitude of the Casimir energy decreases with increasing soliton size. But it also decreases as the stabilizing terms become more important relative to the N$\ell\sigma$ model term.

- With the 1-loop corrections included the $n = 2$ soliton becomes unstable and decays into two individual $n = 1$ solitons (which may still be weakly bound

by a dipole force). We conjecture that the same situation might occur for the 3D-$SU(2)$ $B = 2$ torus in hadron physics.

It is obvious that the program outlined in this paper has to be tailored for specific applications concerning ferromagnets and antiferromagnets. Most importantly for ferromagnets the time derivative part of the lagrangian has to be replaced by the T violating Landau-Lifshitz term with one time derivative only. This replacement may change the results for the Casimir energies appreciably. Also, for antiferromagnets an external magnetic field should couple through the time component of the covariant derivative. Finally, proper consideration of the non–local Coulomb interaction complicates the situation: instead of coupled differential equations coupled integro–differential equations have to be solved for the fluctuations.

The evaluation of loop corrections as presented here naturally suggest the inclusion of temperature into the formalism. This opens the possibility to study the properties of 2D spin–textures at finite temperature, which is of particular interest near the symmetry restoring phase–transition.

This work is supported in parts by funds provided by the FCT, Portugal (Contract PRAXIS/4/4.1/BCC/2753).

Appendix

In this appendix we present analytical soliton solutions for the two limiting cases $a \to 0$ and $a \to \infty$.

Belavin-Polyakov solution for $a \to 0$

The analytical solution of the Euler-Lagrange equation (7) in the limit $a \to 0$

$$\frac{1}{x}\left(xF'\right)' - \frac{n^2 sc}{x^2} = 0 \tag{A.1}$$

with boundary conditions (8) is the well–known Belavin-Polyakov soliton

$$\tan\frac{F}{2} = \left(\frac{b_n}{x}\right)^n . \tag{A.2}$$

The size parameter $b_n^2 = \sqrt{2n(n^2-1)/3}$ is determined by the interplay of the Skyrme- and potential terms contributing to the static energy functional

$$E_n^0 = n + a\,\frac{\pi}{3b_n^2}\,\frac{n^2-1}{\sin\pi/n} + a\,\frac{b_n^2}{2}\,\frac{\pi/n}{\sin\pi/n}\,, \qquad n \neq 1\,. \tag{A.3}$$

The corresponding square radius follows from its definition (5)

$$< x^2 >_n = \sqrt{\frac{2n}{3}(n^2-1)}\,\frac{\pi/n}{\sin \pi/n} \qquad n \neq 1\,. \tag{A.4}$$

It is noticed that in case of the 1-soliton the contribution from the potential term to (A.3) diverges. For that reason we modify (A.2),

$$\tan\frac{F}{2} = b_n \sqrt{\frac{\epsilon}{e^{\epsilon x^2}-1}}\,, \tag{A.5}$$

such that for $\epsilon \to 0$ the Belavin–Polyakov solution is recovered. The variation of the static energy functional in lowest order ϵ

$$E_1^0 = 1 + \frac{\epsilon}{2} + \frac{2a}{3b_1^2} - \frac{ab_1^2}{2}\ell n\epsilon \tag{A.6}$$

gives then $\epsilon = ab_1^2$ and $\ell n\epsilon = -4/3b_1^4$ with the result

$$E_1^0 = 1 + \epsilon(\frac{1}{2} - \ell n\epsilon)\,, \qquad\qquad a^2 = -\frac{3}{4}\epsilon^2 \ell n\epsilon\,. \tag{A.8}$$

Indeed with a also ϵ tends to zero. The square radius behaves like

$$< x^2 >_1 = \sqrt{-\frac{4}{3}\ell n\epsilon} \tag{A.9}$$

and diverges weakly in the limit $a \to 0$. For $a \lesssim 0.001$ the radius of the 1-soliton exeeds that of the 2-soliton. Exactly this behaviour may be traced in the numerical solution if the differential equation (7) is solved for very small a with great precision. Because the square radius (A.9) equals the derivative of the soliton energy with respect to the parameter a, this also explains the infinite slope at the origin indicated in the 1-soliton's curve plotted in Fig. 2.

Solution for $a \to \infty$

The Euler-Lagrange equation (7) in the opposite limit $a \to \infty$

$$\frac{n^2 s}{x}\left(\frac{F's}{x}\right)' - s = 0 \tag{A.10}$$

may also be solved analytically

$$\cos F(x) = \frac{1}{8n^2}(b_n^2 - x^2)x^2 + 2\frac{x^2}{b_n^2} - 1\,, \qquad x \leq b_n\,. \tag{A.11}$$

The integration constants are fixed by the condition $F(b_n) = 0$ connected with topological charge n. The size parameter $b_n^2 = 4n$ again minimizes the static energy functional

$$E_1^0 = na \left[\frac{b_n^2}{4n} + \frac{1}{2} \left(\frac{4n}{b_n^2} \right) - \frac{1}{6} \left(\frac{b_n^2}{4n} \right)^3 \right] \tag{A.12}$$

with the results quoted in (9)

$$E_n^0 = \frac{4n}{3} a \,, \qquad\qquad < x^2 >_n = \frac{4n}{3} \,. \tag{A.13}$$

Needless to say, that numerical solutions of the Euler-Lagrange equation (7) reproduce these results for large enough a.

References

[1] S.L. Sondhi, A. Karlhede, and S.A. Kivelson, Phys. Rev. **B47**, 16419 (1993).

[2] I. Dzyaloshinskii, A. Polyakov and P. Wiegmann, Phys. Lett. **A127**, 112 (1988).

[3] M. Abolfath, cond-mat/9712260.

[4] J.P. Rodriquez, Phys. Rev. **B39**, 2906 (1989).

[5] R.F. Dashen, B. Hasslacher and A. Neveu, Phys. Rev. **D10**, 4114, 4130 (1974).

[6] D. Lilliehook, K. Lejnell, A. Karlhede, and S.L. Sondhi, cond-mat/9704121.

[7] Yu.V. Nazarov and A.V. Khaetskii, Phys. Rev. Lett. **80**, 576 (1998).

[8] C.P. Burgess, hep-th/9808176.

[9] C.P. Hofmann, cond-mat/9805277.

[10] J.M. Roman and J. Soto, Int. J. Mod. Phys. **B3**, 755 (1999).

[11] K. Moon and K. Mullen, cond-mat/9707250.

[12] A.A. Belavin and A.M. Polyakov, JETP Lett. **22**, 245 (1975).

[13] B.M.A.G. Piette, B.J. Schroers, and W.J. Zakrzewski, Z. Phys. **C65**, 165 (1995); Nucl. Phys. **B439**, 205 (1995).

[14] B.A. Ivanov, A.K. Kolezhuk, and G.M. Wysin, Phys. Rev. Lett. **76**, 511 (1996).

[15] B.A. Ivanov, H.J. Schnitzer, F.G. Mertens, and G.M. Wysin, cond-mat/9805177.

[16] A.M. Polyakov, Phys. Lett. **59B**, 79 (1975).

[17] C.G. Callan and I. Klebanov, Nucl. Phys. **B262**,365 (1985).

[18] P.M. Morse and H. Feshbach, *Methods of Theoretical Physics*, McGraw Hill, N.Y. (1953) Ch. 11.2.

[19] H. Walliser and G. Eckart, Nucl. Phys. **A429**, 514 (1984).

[20] B. Moussallam, Ann. Phys. **225**, 264 (1993).

[21] F. Meier and H. Walliser, Phys. Rep. **289**, 383 (1997).

[22] C.G. Bollini and J.J. Giambiagi, Phys. Lett. **40B**, 566 (1972), Nuovo Cim. **12B**, 20 (1972); G. 'tHooft and M. Veltmann, Nucl. Phys. **B44**, 189 (1972).

[23] C.G. Bollini and J.J. Giambiagi, Nuovo Cim. **93A**, 113 (1986).

[24] C.P. Martin, Phys. Lett. **B241**, 513 (1990); R. Delbourgo and A.B. Waites, Phys. Lett. **B300**, 241 (1993).

[25] G. Ecker, in Proc. of 5th Workshop on Hadron Physics, Angra dos Reis, RJ, Brasil, 1996.

[26] M. Abolfath, J.J. Palacios, H.A. Fertig, S.M. Gervin and A.H. MacDonald, Phys. Rev. **B56**, 6795 (1997).

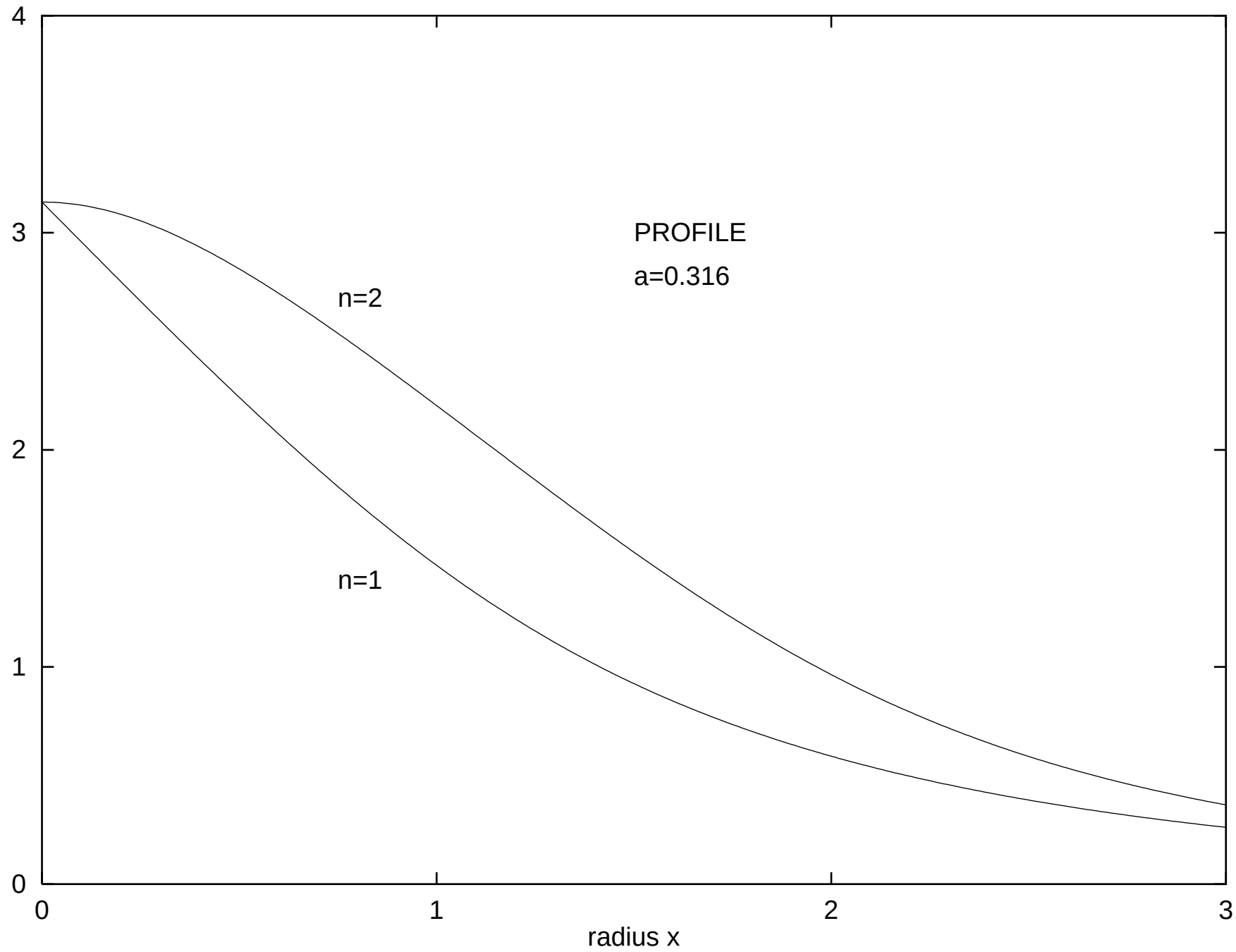
PROFILE
a=0.316
n=2
n=1
4
3
2
1
0
0
1
2
3
radius x

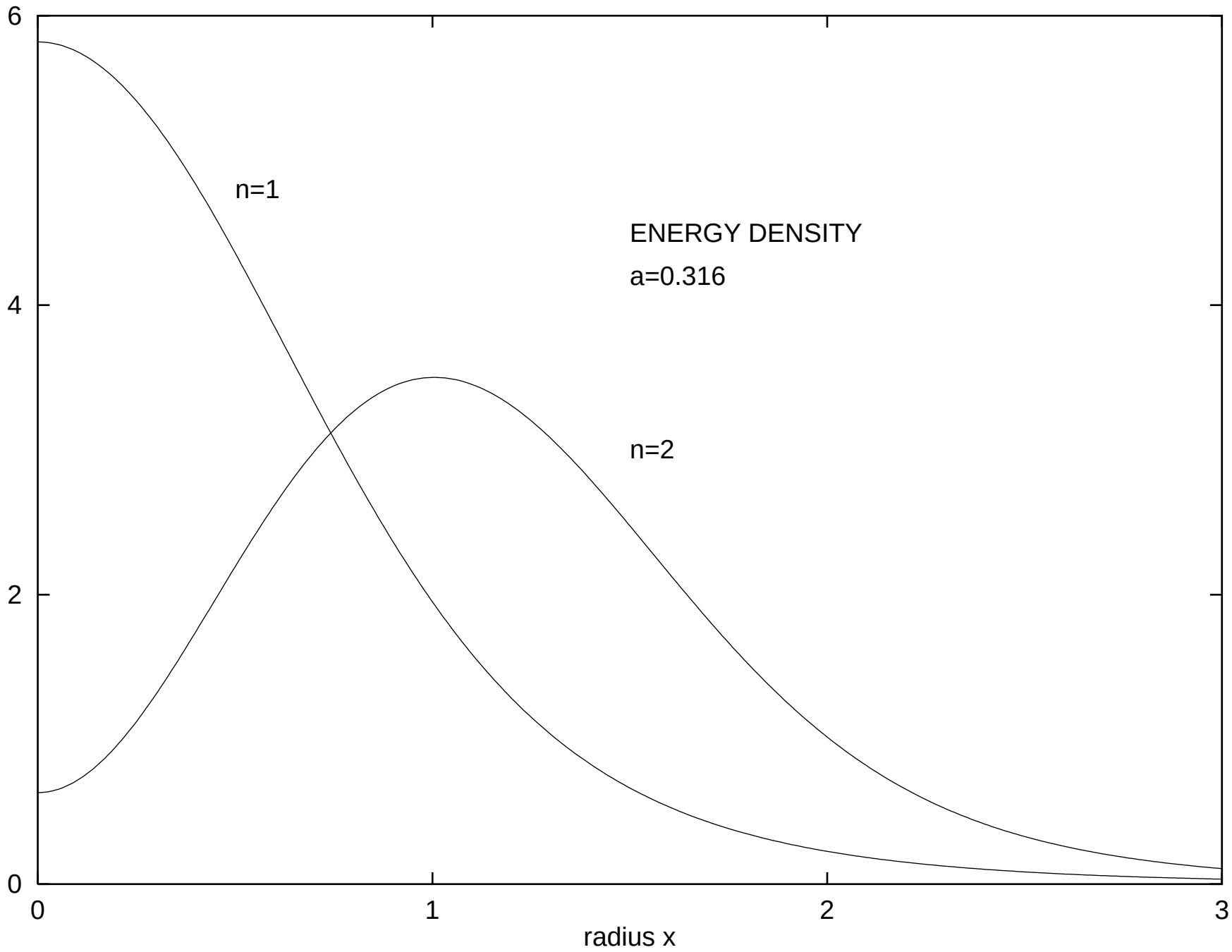
6
4
2
0
0
1
2
3
radius x
n=1
n=2
ENERGY DENSITY
a=0.316